ChemComm

COMMUNICATION

View Article Online
View Journal



Cite this: DOI: 10.1039/d6cc02773c

Received 4th May 2026,
Accepted 16th May 2026

DOI: 10.1039/d6cc02773c

rsc.li/chemcomm

# A new cation- and vacancy-ordered brownmillerite in the Ba–In–Fe–O system revealing hidden order in its cubic counterpart

Monica Ceretti, *[a] Gabriel J. Cuello, [b] Denis Sheptyakov, [c] Anna Marsicano[d] and Werner Paulus [a]

**The synthesis and characterization of a previously unreported B-cation ordered $Ba_2InFeO_5$ brownmillerite, obtained by an unconventional ultra-high-vacuum method, are reported alongside its cubic perovskite-type counterpart. Neutron diffraction and total scattering studies reveal for both phases ordered oxygen vacancies together with a layered $FeO_4/InO_6$ leitmotif, which gives rise to suppressed magnetic susceptibility and low-dimensional magnetic behavior. This work shows that ultra-high vacuum synthesis allows B-cation ordering to get stabilized forming new brownmillerite type oxides, establishing $Ba_2InFeO_5$ as a model system for studying isolated 1D-tetrahedral $Fe^{3+}$ chains, magnetic frustration, and structure–magnetism relationships.**

Brownmillerite oxides, with general formula $A_2BB'O_5$, form an important family of oxygen-deficient perovskites characterised by the ordered layering of $BO_6$ octahedra and $BO_4$ tetrahedra, a motif enabled by a flexible oxygen-vacancy lattice. The assignment of the space group often remains ambiguous due to subtle structural changes, making it difficult to differentiate between different types of tetrahedral chain ordering and their corresponding space group symmetries, such as *Pnma*, *Imma*, and *I2mb*.[1,2] Reorganization of the vacancy network under different thermodynamic conditions enables oxygen-deficient perovskites to access cubic or brownmillerite polymorphs depending on the synthesis route; however, the simultaneous occurrence of both polymorphs within a single material is uncommon.[3,4]

$Ba_2In_2O_5$ is a well-known prototypical brownmillerite, characterized by long-range ordered oxygen vacancies and alternating layers of $InO_6$ octahedra and $InO_4$ tetrahedra.[5,6] It has been widely studied for its high oxide-ion and proton conductivity, making it a promising electrolyte for solid oxide fuel cells, oxygen-generation systems, and dense catalytic membranes.[6–11] Many elemental substitutions have been attempted in order to improve its conductivity. Ga substitution in $Ba_2(In_{1-x}Ga_x)_2O_5$ modifies the structure from orthorhombic brownmillerite ($x < 0.3$) to cubic perovskite ($0.3 < x < 0.5$), while for $x = 0.5$, it adopts a cation-ordered brownmillerite structure with layered In octahedra and Ga tetrahedra.[12,13] Substitution of $In^{3+}$ with transition-metal cations (MT) with multiple accessible oxidation states and coordination environments, strongly perturbs the vacancy and thus the physical properties.[14] High levels of doping in $Ba_2In_{2-x}M_xO_5$ (with $x > 0.2$) and fluorine intercalation are known to stabilize a defect cubic perovskite structure.[14–17] An extensive study has investigated the corresponding Fe-doped analogous cubic oxygen deficient perovskite $Ba_2In_{2-x}Fe_xO_5$.[15] Despite this, the vacancy-ordered brownmillerite derivatives of these systems remain largely unexplored. Here, we report the synthesis and a comprehensive characterization of a new brownmillerite phase, $Ba_2InFeO_5$, obtained under ultra-high vacuum (UHV) and stabilized *via* Fe/In cation ordering. Thus, this work provides the first detailed insight into the structural ordering and magnetic behaviour of this previously unreported phase, highlighting the potential of cation ordering as a strategy for stabilizing novel oxide frameworks. Moreover, by probing both polymorphs, cubic and brownmillerite, *via* neutron pair distribution function analysis, we uncover key similarities in their local structures.

Brownmillerite $Ba_2InFeO_5$ (BFIO-BM in the following) was obtained by annealing the cubic perovskite precursor (BFIO-C in the following) at 1273 K under UHV conditions for several days. The BFIO-C precursor itself was prepared by high-temperature solid-state reaction of stoichiometric $In_2O_3$, $Fe_2O_3$ and $BaCO_3$ under flowing Ar. Full synthesis details are provided in the SI.

Laboratory powder X-ray diffraction (PXRD) patterns were collected using a Panalytical X'pert Pro diffractometer and neutron powder diffraction (NPD) data were measured with the HPRT powder diffractometer[18] at SINQ spallation neutron source of the Paul Scherrer Institute (CH), while neutron total scattering data were collected on the disorder materials diffractometer D4c at the ILL (Grenoble).[19,20] Magnetization was measured using a

[a] *ICGM, Univ Montpellier, CNRS, ENSCM, 34000 Montpellier, France. E-mail: monica.ceretti@umontpellier.fr*
[b] *Institut Laue-Langevin, 38042 Grenoble, France*
[c] *PSI, Center for Neutron and Muon Sciences, Villigen CH-5232, Switzerland*
[d] *ISIS Neutron and Muon Facility, Rutherford Appleton Laboratory, Chilton, OX11 OQX, UK*

SQUID magnetometer (further details for experimental methods are given in the SI).

Powder X-ray diffraction (PXRD) confirmed that the BFIO-C precursor adopts the expected cubic oxygen-deficient perovskite structure, in agreement with previous reports in the literature,[15] well indexed in the $Pm\bar{3}m$ space group with $a$ = 4.1562 (2) Å (Fig. S1a). After a 4-days annealing treatment at 1273 K in UHV, the material undergoes a complete transformation to the brownmillerite phase BFIO-BM. PXRD (Fig. S1b) confirms the phase purity of the annealed material, with no detectable impurity phases and lattice parameters $a$ = 5.9410 (4) Å, $b$ = 15.7331 (10) Å, and $c$ = 6.1009 (4) Å. The average and local structure was studied in more detail by neutron diffraction. Assigning the correct space group in brownmillerite-type structures is challenging because ordered and disordered chain arrangements can produce nearly indistinguishable diffraction patterns. Here, PXRD and neutron powder diffraction (NPD) alone did not allow unambiguously to discriminate between the *I2mb* and *Imma* models, both of which give comparably good refinements (Fig. 1 and Fig. S2), while the

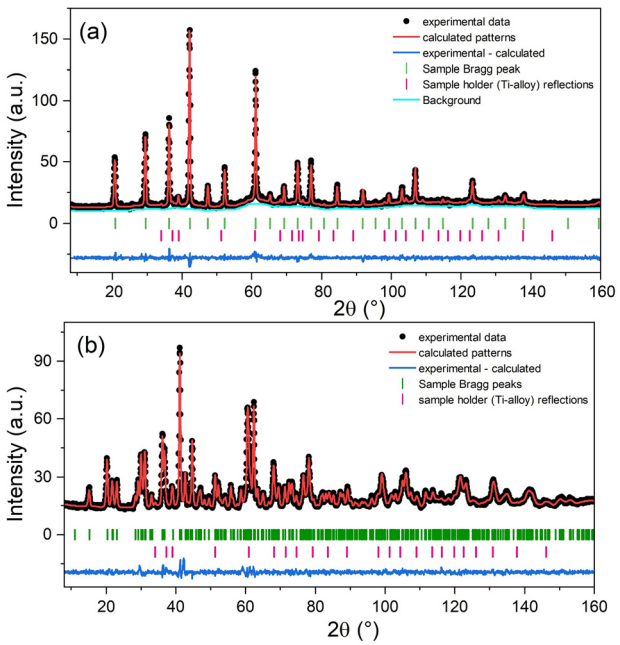


Fig. 1 Rietveld refinements of NPD data at RT of (a) the cubic $Pm\bar{3}m$ oxygen deficient perovskite BFIO-C and (b) of the orthorhombic *I2mb* brownmillerite BFIO-BM. The cyan line in (a) represents the background, in which modulations can be observed.

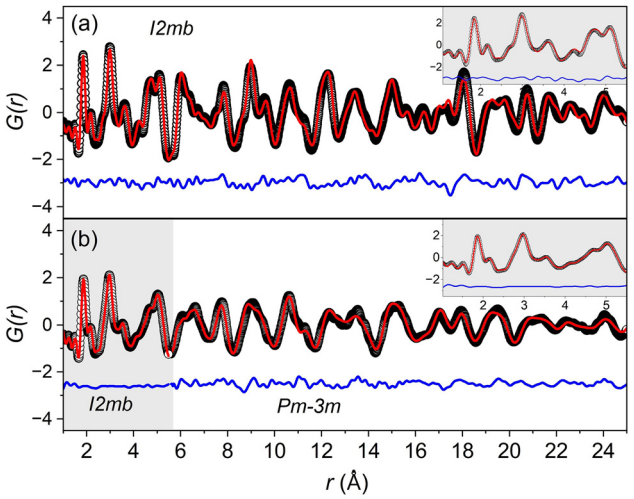


Fig. 2 (a) PDFgui refinement of orthorhombic BFIO-BM (*I2mb*) over $r$ = 1–25 Å ($R_w$ = 15%). (b) Short- and long-range $G(r)$ of BFIO-C refined with *I2mb* for 1–5 Å and $Pm\bar{3}m$ for higher $r$; inset shows short-range region. Black open circles are the experimental data and the red line is the profile fitting, while the blue line is the difference.

*Pnma* was excluded as no *I*-centering–forbidden reflections were detected. However, pair distribution function (PDF) analysis of BFIO-BM reveals that both the average and local structures are well described by the *I2mb* symmetry (fitting residuals $R_w$ = 15%, Fig. 2a and Table S3, SI), whereas the *Imma* model fails to provide an adequate fit to the PDF data ($R_w$ = 43%, Fig. S3). Accordingly, neutron powder diffraction (NPD) Rietveld refinements were subsequently performed in the *I2mb* space group (Fig. 1a), and the refined atomic coordinates are summarized in Table 1. The refined site occupancies confirm that, within experimental uncertainty, the tetrahedral sites are exclusively occupied by Fe, while In occupies the octahedral sites, providing compelling evidence for long-range cation ordering in BFIO-BM. Bond distances (reported in Table S2) indicate that the $InO_6$ octahedron is slightly distorted due to the structural connectivity, with In–O bond lengths ranging from 2.13–2.30 Å, although the O–In–O bond angles remain close to 90° and 180°, in line with values reported for a related brownmillerite oxide.[13] The $FeO_4$ tetrahedra are significantly distorted, exhibiting a widened O–Fe–O angle of up to 130°, while the remaining bond angles fall in the range 102–108°. The Fe–O bond lengths split into two distinct values (1.85 Å and 1.91 Å), indicating a quite pronounced deviation from ideal tetrahedral geometry. The calculated bond valence sums (BVS) for each ion (Table 1)

Table 1 Crystal structure parameters of BFIO-BM obtained from Rietveld neutron data refinements against the *I2mb* space group. Lattice parameters: $a$ = 5.9410 (4) Å, $b$ = 15.7331 (10) Å, $c$ = 6.1009 (4) Å ($R_p$ = 2.74%; $R_{wp}$ = 3.65%; $R_{Bragg}$ = 2.16%, $R_f$ = 1.8%, $\chi^2$ = 1.84). Data obtained on HRPT at PSI ($\lambda$ = 1.494 Å)

| Atom | $x$ | $y$ | $z$ | $U_{iso}$ (Å$^2$) | Occ. | Site | BVS |
|---|---|---|---|---|---|---|---|
| Ba | 0.5066 (25) | 0.8824 (2) | 0.0026 (5) | 0.0058 (7) | 1.0 | 8*c* | 1.93 (3) |
| Fe | 0.0108 (21) | 0.25 | 0.0613 (4) | 0.0072 (7) | 0.98 (7) | 4*a* | 2.98 (6) |
| In | 0.00 | 0.00 | 0.00 | 0.0124 (16) | 1.02 (7) | 4*b* | 2.80 (4) |
| O1 | 0.2498 (3) | 0.0117 (2) | 0.2516 (2) | 0.0100 (8) | 1 | 8*c* | 2.03 (3) |
| O2 | 0.0225 (16) | 0.8563 (2) | 0.0694 (5) | 0.0122 (9) | 1 | 8*c* | 1.76 (7) |
| O3 | 0.7692 (22) | 0.75 | 0.7316 (2) | 0.0120 (16) | 0.97 (5) | 4*b* | 2.07 (3) |

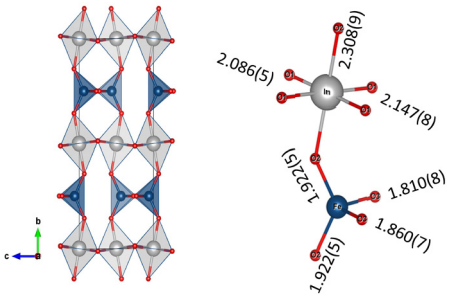


Fig. 3 BFIO-BM brownmillerite structure with oxygen-vacancy layers forming alternating $InO_6$ (gray) and $FeO_4$ (blue) chains in *I2mb* symmetry (Ba omitted). Schematic of polyhedra and bond lengths obtained from PDF refinement. Structure drawn with VESTA.[19]

are close to their expected formal valence states, supporting the assignment of $Fe^{3+}$ and being consistent with oxygen stoichiometry. Overall, for BFIO-BM, the structures refined from PDF and NPD analyses are consistent within the experimental uncertainties. In addition, PDF results show no evidence of short-range disorder, with only minor variations in the In–O bond distances (Fig. 3). On the other hand, several oxygen-deficient perovskite polymorphs, both cubic and brownmillerite, have been shown to often preserve an ordered oxygen-vacancy configuration.[3,4,21–24] Consistent with this picture, some modulations in the diffuse background of the neutron powder diffraction pattern are observed for BFIO-C (Fig. 1a), which are absent in the X-ray diffraction data and are indicative of local structural correlations beyond the average crystallographic model. A possible origin of this behaviour can be found in the twin-domain complexity of perovskite-related oxides. Indeed, nanoscopic intergrowths comprising up to twelve distinct orthorhombic twin domains have previously been reported within structures that appear macroscopically cubic.[25] Thus, the superposition of multiple twin domains in cubic BFIO-C can account for the unusually large atomic displacement parameters refined for all atoms in the Rietveld analysis (Fig. S8 and Table S4).

Fig. S4 presents the neutron PDF $G(r)$ in the nearest-neighbour region (1 Å $< r <$ 4.5 Å) for both BFIO-BM and the nominally cubic BFIO-C phases at room temperature. For reference, the interatomic distances, expected for an average cubic perovskite model ($Pm\bar{3}m$, $a$ = 4.1562 (2) Å), are indicated by dashed lines. For BFIO-C, the first two prominent peaks, corresponding to (Fe/In)–O and Ba–O nearest-neighbour distances, are clearly splited and closely resemble those observed for BFIO-BM. This demonstrates that, despite the apparent average cubic symmetry of BFIO-C, the local coordination environment is highly distorted and closely related to that of the brownmillerite phase. At shorter length scales ($r \lesssim 5$ Å), the experimental $G(r)$ is therefore better described by a brownmillerite-like local structure (inset Fig. 2b), reflecting locally ordered oxygen vacancies and alternating coordination geometries. PDF analysis assuming cationic disorder (*i.e.*, sites occupied by 50% In and 50% Fe), however, fails to fit the experimental data (see Fig. S5), whereas a local Fe/In ordering can be nicely fitted in the low-$r$ region, confirming for the first time a B-cation order despite the average cubic symmetry. Only at larger interatomic distances, the PDF gradually converge toward the average cubic description, indicating that long-range disorder averages out these local distortions (Fig. 2b). This crossover from local brownmillerite-like order to average cubic symmetry highlights the coexistence of short-range order with long-range disorder. Importantly, this local structural behaviour implies a layered sequence of alternating $InO_6$ octahedra and $FeO_4$ tetrahedra, characteristic of brownmillerite-type vacancy ordering. Previous X-ray PDF investigations of $BaIn_{0.5}Fe_{0.5}O_{2.5}$ have already revealed deviations from ideal cubic $Pm\bar{3}m$ symmetry at short range, pointing to local structural heterogeneity.[15] They were, however, insufficient to determine Fe/In cation ordering. In the present work, neutron PDF analysis provides a clearer picture of local distortions. Although Fe and In have comparable scattering contrast in X-rays and neutrons (with reversed ratio), neutrons benefit from **Q**-independent scattering lengths, enabling reliable high-Q data and higher real-space resolution. As shown in Fig. S7, only neutron PDF data can clearly distinguish between ordered and disordered B-site cation arrangements. Thus, neutron PDF results provide compelling evidence for B-site cation ordering together with oxygen-vacancy ordering persisting over short length scales in both BFIO-BM and BFIO-C.

Fig. 4a displays the temperature dependence of the DC magnetic susceptibility of BFIO-BM, under field-cooled (FC) and zero-field-cooled (ZFC) conditions. Measurements were performed between 2 and 300 K in an applied field of 1000 Oe, with ZFC data extended up to 400 K. Neither FC nor ZFC data show signatures of long-range magnetic ordering down to 2 K. The BM phase shows overall lower susceptibility values compared to the cubic phase (Fig. S6), whose magnetic behaviour is consistent with previous reports.[15] Field-dependent magnetization (Fig. 4b), measured at 300 and 15 K over ±50 kOe, reveals linear behaviour at 300 K, indicative of paramagnetism. At 15 K, the M(H) curve remains nearly linear across the full field range, with no hysteresis or saturation; only a slight low-field curvature is observed, possibly indicating the presence of magnetic correlations. The temperature-dependent magnetic susceptibility of $Ba_2InFeO_5$ exhibits a linear $\chi^{-1}$ *vs.* $T$ relationship above 290 K, indicative of paramagnetic behaviour, while deviations occur at lower temperatures. A Curie–Weiss analysis was therefore restricted to the high-temperature region ($T \geq$ 290 K), where the extracted effective magnetic

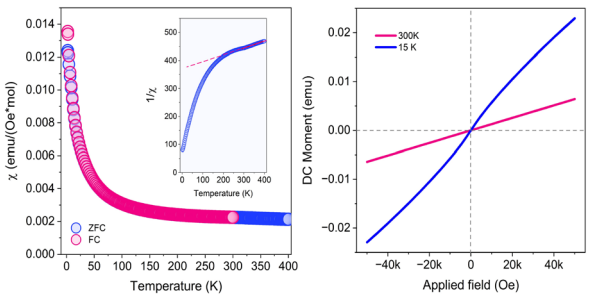


Fig. 4 (a) Temperature dependence of the field-cooled (red dots) and the zero-field-cooled (blue dots) molar magnetic susceptibility ($\chi$) of BFIO-BM. The inverse susceptibility $1/\chi$, shown in the inset, is fitted with the Curie–Weiss law (red line) in the 290–300 K interval. (b) Magnetisation field loops at 15 K and 300 K.

moment (5.65 ± 0.7)$\mu_B$ is close to the spin-only value for $Fe^{3+}$ ($S$ = 5/2, $\mu_{eff}$ = 5.9$\mu_B$), although the restricted temperature interval used for the fit inherently limits the precision. The deviation from Curie–Weiss behaviour at lower temperatures indicates the development of short-range magnetic interactions, which likely hinder long-range ordering and suggest low-dimensional magnetic behaviour. Such magnetic properties are consistent with previous reports on $Sr_2ScFeO_5$, the only brownmillerite phase so far reported in the literature where $Fe^{3+}$ exclusively occupies tetrahedral sites.[3] The absence of long-range magnetic order, despite local interactions, highlights the influence of the brownmillerite framework, where alternating FeO and $InO_2$ layers spatially isolate magnetic exchange pathways. These results emphasize how cation ordering and coordination geometry govern magnetic dimensionality, providing a platform for exploring low-dimensional magnetism in complex oxides. This magnetic behaviour can be understood in terms of the brownmillerite crystal structure, which consists of alternating magnetic FeO layers and non-magnetic $InO_2$ layers, with an average separation between adjacent FeO layers of about 8 Å. Moreover, Rietveld refinements reveal distorted $FeO_4$ tetrahedra, modifying Fe–O–Fe bond angles and thus super-exchange interactions. These features are expected to weaken interlayer coupling and promote reduced magnetic dimensionality. Although the presence of minor magnetic impurities cannot be completely ruled out, both PXRD (Fig. S1b) and M(H) measurements suggest that any secondary phases lie below the ~1% detection limit, supporting an intrinsic origin for the observed magnetic behaviour.

In conclusion, this work reports the first synthesis and comprehensive characterization of the brownmillerite-type $Ba_2InFeO_5$. In contrast to previously studied Fe-doped $Ba_2In_2O_5$ systems,[15] which adopt the defect-cubic form at high Fe content, $Ba_2InFeO_5$ represents a fully ordered Fe/In brownmillerite stabilised under ultra-high vacuum conditions. The exclusive occupation of $Fe^{3+}$ in the tetrahedral sites leads to the formation of structurally isolated 1D-$FeO_4$ chains, in contrast to the mixed coordination environments typically observed in related systems.[26–30] This unique structural configuration gives rise to a strongly suppressed and low dimensional magnetic response. Detailed neutron diffraction and pair distribution function analyses provide compelling evidence for both long- and short-range ordering of oxygen vacancies together with B-site cations for both, the brownmillerite and, for the first time, in the perovskite-type polymorph. Together with neutron PDF analysis, these results show that targeted synthesis can stabilize unconventional cation orderings and extend brownmillerite-related structures beyond conventional limits.

## Conflicts of interest

There are no conflicts to declare.

## Data availability

The data supporting this article have been included as part of the supplementary information (SI). Supplementary information: sample preparation, powder X-ray diffraction, powder neutron diffraction, structural model and magnetic measurement. Neutron total scattering data obtained on D4c at the ILL are available through https://doi.ill.fr/10.5291/ILL-DATA.6-06-532. See DOI: https://doi.org/10.1039/d6cc02773c.

## Acknowledgements

This work is partly based on experiments performed at the Swiss spallation neutron source, PSI, Villigen (CH). Beam time allocation on D4c at the ILL (Grenoble) and HRPT at SINQ is gratefully acknowledged. The authors thank the ''Plateforme d'Analyse et de Caractérisation'' of the ICGM for support with XRD and magnetization measurements.

## References

1 T. G. Parsons, H. D'Hondt, J. Hadermann and M. A. Hayward, *Chem. Mater.*, 2009, **21**, 5527–5538.
2 A. M. Abakumov, A. M. Alekseeva, M. G. Rozova, E. V. Antipov, O. I. Lebedev and G. V. Tendeloo, *J. Solid State Chem.*, 2003, **174**, 319–328.
3 S. Marik, B. Gonano, F. Veillon, Y. Bréard, D. Pelloquin, V. Hardy, G. Clet and J. M. Le Breton, *Chem. Commun.*, 2019, **55**, 10436–10439.
4 M. Ceretti, G. Agostini, M. Brunelli, S. Corallini, G. Perversi, G. Cuello, A. Marsicano and W. Paulus, *Inorg. Chem.*, 2020, **59**, 9434–9442.
5 A. Mancini, J. F. Shin, A. Orera, P. R. Slater, C. Tealdi, Y. Ren, K. L. Page and L. Malavasi, *Dalton Trans.*, 2012, **41**, 50–53.
6 S. Speakman, *Solid State Ionics*, 2002, **149**, 247–259.
7 J. Goodenough, *Solid State Ionics*, 1990, **44**, 21–31.
8 T. Schober and J. Friedrich, *Solid State Ionics*, 1998, **113–115**, 369–375.
9 T. Schober, J. Friedrich and F. Krug, *Solid State Ionics*, 1997, **99**, 9–13.
10 K. Nakagawa, A. Iwase and A. Kudo, *Chem. Lett.*, 2018, **47**, 1526–1529.
11 A. Rolle, N. V. Giridharan, P. Roussel, F. Abraham and R.-N. Vannier, *MRS Proc.*, 2004, **835**, K2.4.
12 T. Yao, Y. Uchimoto, M. Kinuhata, T. Inagaki and H. Yoshida, *Solid State Ionics*, 2000, **132**, 189–198.
13 C. Didier, J. Claridge and M. Rosseinsky, *J. Solid State Chem.*, 2014, **218**, 38–43.
14 P. Jiang, J. Li, A. Ozarowski, A. W. Sleight and M. A. Subramanian, *Inorg. Chem.*, 2013, **52**, 1349–1357.
15 A. D. Lozano-Gorrín, B. Wright, P. A. Dube, C. A. Marjerrison, F. Yuan, G. King, D. H. Ryan, C. Gonzalez-Silgo, L. M. D. Cranswick, A. P. Grosvenor and J. E. Greedan, *ACS Omega*, 2021, **6**, 6017–6029.
16 S. Chaoudhary, L. Nguyen, X. Xiao, A. Weidenkaff, A. Klein and M. Widenmeyer, *Chem. Mater.*, 2025, **37**, 1621–1628.
17 G. S. Case, A. L. Hector, W. Levason, R. L. Needs, M. F. Thomas and M. T. Weller, *J. Mater. Chem.*, 1999, **9**, 2821–2827.
18 P. Fischer, G. Frey, M. Koch, M. Könnecke, V. Pomjakushin, J. Schefer, R. Thut, N. Schlumpf, R. Bürge, U. Greuter, S. Bondt and E. Berruyer, *Phys. B*, 2000, **276–278**, 146–147.
19 M. Ceretti, G. Cuello and W. Paulus, Exploring Proton Conductivity Mechanisms In Oxygen Deficient Perovskites $SrSc_{0.5}Ga_{0.5}O_{2.5}$, Institut Laue-Langevin (ILL), 2024, DOI: 10.5291/ILL-DATA.6-06-532.
20 H. E. Fischer, G. J. Cuello, P. Palleau, D. Feltin, A. C. Barnes, Y. S. Badyal and J. M. Simonson, *Appl. Phys. A: Mater. Sci. Process.*, 2002, **74**, s160–s162.
21 G. King, F. Ramezanipour, A. Llobet and J. E. Greedan, *J. Solid State Chem.*, 2013, **198**, 407–415.
22 G. King, C. M. Thompson, K. Luo, J. E. Greedan and M. A. Hayward, *Dalton Trans.*, 2017, **46**, 1145–1152.
23 F. Ramezanipour, J. E. Greedan, J. Siewenie, R. L. Donaberger, S. Turner and G. A. Botton, *Inorg. Chem.*, 2012, **51**, 2638–2644.
24 F. Ramezanipour, J. E. Greedan, J. Siewenie, T. Proffen, D. H. Ryan, A. P. Grosvenor and R. L. Donaberger, *Inorg. Chem.*, 2011, **50**, 7779–7791.

 

25 A. Maity, R. Dutta, B. Penkala, M. Ceretti, A. Letrouit-Lebranchu, D. Chernyshov, A. Perichon, A. Piovano, A. Bossak, M. Meven and W. Paulus, *J. Phys. D: Appl. Phys.*, 2015, **48**, 504004.
26 Q. E. Stahl, G. J. Redhammer, G. Tippelt and A. Reyer, *Phys. Chem. Miner.*, 2019, **46**, 271–298.
27 F. Ramezanipour, J. E. Greedan, A. P. Grosvenor, J. F. Britten, L. M. D. Cranswick and V. O. Garlea, *Chem. Mater.*, 2010, **22**, 6008–6020.
28 K. Nakayama, R. Ishikawa, A. Kuwabara, S. Kobayashi, T. Motohashi, N. Shibata and Y. Ikuhara, *Inorg. Chem.*, 2019, **58**, 10209–10216.
29 A. P. Grosvenor and J. E. Greedan, *J. Phys. Chem. C*, 2009, **113**, 11366–11372.
30 H. D'Hondt, A. M. Abakumov, J. Hadermann, A. S. Kalyuzhnaya, M. G. Rozova, E. V. Antipov and G. Van Tendeloo, *Chem. Mater.*, 2008, **20**, 7188–7194.